

Unraveling the Physicochemical Determinants of Protein Liquid-liquid Phase Separation by Nanoscale Infrared Vibrational Spectroscopy

Francesco S. Ruggeri^{1, 2, §, *}, Alyssa M. Miller¹, Michele Vendruscolo¹ and Tuomas P. J. Knowles^{1, 3}

¹Laboratories of Organic and Physical Chemistry, Stippeneng 4, 6703 WE, Wageningen University and Research, The Netherlands. ²Department of Chemistry, University of Cambridge, Cambridge, UK; ³Cavendish Laboratory, University of Cambridge, Cambridge, UK; [§]Present address: Helix Building, 6708 WE, Wageningen, The Netherlands

*For correspondence: simone.ruggeri@wur.nl

[Abstract] The phenomenon of reversible liquid-liquid phase separation of proteins underlies the formation of membraneless organelles, which are crucial for cellular processes such as signalling and transport. In addition, it is also of great interest to uncover the mechanisms of further irreversible maturation of the functional dense liquid phase into aberrant insoluble assemblies due to its implication in human disease. Recent advances in methods based on atomic force microscopy (AFM) have made it possible to study protein condensates at the nanometer level, providing unprecedented information on the nature of the intermolecular interactions governing phase separation. Here, we provide an in-depth description of a protocol for the characterisation of the morphology, stiffness, and chemical properties of protein condensates using infrared nanospectroscopy (AFM-IR).

Keywords: Liquid-liquid phase separation, Infrared nanospectroscopy, Atomic force microscopy, Single-molecule biophysics

[Background] Liquid-liquid phase separation (LLPS, Figure 1) is a fundamental process resulting in the formation of membraneless subcellular bodies, such as nucleoli and germ granules (Hyman *et al.*, 2014; Banani *et al.*, 2017). This reversible transition, during which proteins condense into a dense liquid phase or droplet within the cell, is involved in many aspects of cellular organisation and function, such as mRNA processing and signalling (Murakami *et al.*, 2015). It has been realised that most of the proteins that undergo LLPS contain intrinsically disordered domains (IDRs), which are involved in networks of multivalent interactions that underpin the condensation process (Li *et al.*, 2012). However, dysregulation of this process can lead to the formation of solid hydrogel-like inclusions, which are implicated in human disease. Such is the case of fused in sarcoma (FUS), an RNA-binding protein implicated in the onset of amyotrophic lateral sclerosis (ALS) and frontotemporal dementia (FTD) (Patel *et al.*, 2015).

The LLPS behaviour of protein condensates has typically been studied using optical and fluorescence microscopy methods, as well as bulk characterisation of properties in solution, such as turbidity measurements (Alberti *et al.*, 2019). These approaches have shown the effect of external factors on the modulation of phase separation, revealing the influence of protein concentration, pH, salt type and concentration, and small molecules (Hyman *et al.*, 2014; Murakami *et al.*, 2015; Patel *et al.*, 2017; Ruggeri *et al.*, 2018; Alberti *et al.*, 2019). A further understanding of the process of LLPS, in particular

the fundamental molecular interactions determining protein condensation and the inner structure of the individual protein condensates, is hampered by their intrinsic transient nature and sub-micrometer scale dimensions. However, conventional approaches, which are limited by their spatial resolution and the need for highly concentrated samples, cannot probe molecular mechanisms and internal factors determining LLPS at the individual condensate and sub-condensate levels.

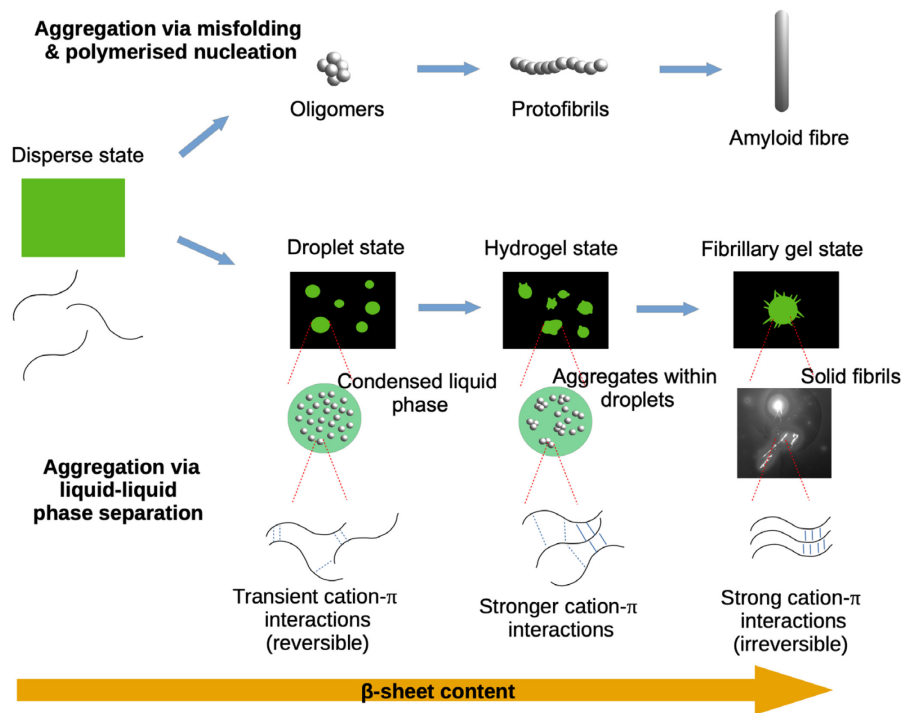


Figure 1. Schematic of protein aggregation vs. liquid-liquid phase separation and liquid-to-solid transition

In our previous and current work (Müller *et al.*, 2014; Ruggeri *et al.*, 2015, 2016a, 2018, 2020a, and 2020b; Ramer *et al.*, 2018; Lipiec *et al.*, 2019), we have demonstrated that infrared nanospectroscopy (AFM-IR) can provide new and complementary information, as compared with bulk methods, regarding the phenomenon of protein LLPS at the sub-condensate nanoscale level. This information can then be successfully exploited to address fundamental knowledge gaps in the physicochemical determinants of this process (Müller *et al.*, 2014; Ruggeri *et al.*, 2015, 2016a, 2016b, 2018, 2020a; Dazzi and Prater, 2017; Lipiec *et al.*, 2019). AFM-IR combines the capabilities of infrared spectroscopy (IR) and atomic force microscopy (AFM) to allow for the simultaneous characterisation of morphology, stiffness, and chemical properties of individual droplets, and even of different regions within the same droplet, thereby providing mechanistic insight into their inner biophysical properties and formation.

The AFM-IR system bases its function on scanning probe microscopy (Figure 2). Briefly, during morphology acquisition, the tip and cantilever in contact with the sample can be used to acquire nanomechanical and nanospectroscopy information. The relative stiffness of the sample is evaluated by considering the tip and the sample in contact as a system of coupled springs. The contact resonance

frequency of these springs is monotonically related to the intrinsic stiffness of the sample (Volpatti *et al.*, 2016; Qamar *et al.*, 2018). A stiffer sample would cause an increase in contact resonance, which we can term 'frequency shift'; thus, the mechanical properties at the sub-droplet nanoscale level can be measured (Qamar *et al.*, 2018; Shen *et al.*, 2020). To retrieve chemical information in the form of nanoscale-resolved maps and localised spectra, the tip is used as a detector of photothermal expansion. If a sample absorbs IR light at a specific wavelength, the chemical bonds absorbing the light will vibrate; this vibration is dissipated as thermal heat, producing a sample expansion that can be measured by the AFM tip in contact with the sample. The response of the cantilever is proportional to the IR absorption (Ruggeri *et al.*, 2016b). Localised IR spectra can be acquired by holding the tip at a fixed position on the sample while sweeping the frequency of the IR light. Similarly, IR maps of whole droplets can also be acquired by measuring the thermal expansion at a fixed wavelength during the measurement of sample morphology. AFM-IR is capable of acquiring chemical information down to the single protein molecule scale (Ruggeri *et al.*, 2020a). In the case of LLPS of proteins, it is relevant to investigate the vibrations associated with the amide band I, which is related to C=O stretching (80%) and is therefore sensitive to the conformation and hydrogen bonding of the protein backbone. Thus, the shape of the amide band I is studied to reveal secondary and quaternary structural information (Ruggeri *et al.*, 2015; 2016a and 2020a).

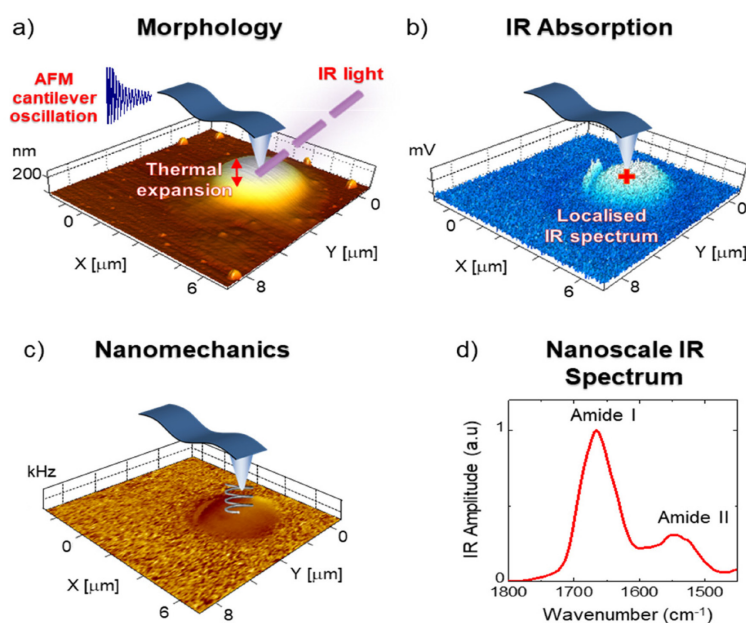


Figure 2. AFM-IR nanoscale chemical imaging and spectroscopy principles for a liquid-liquid phase-separated droplet. Absorbed IR light causes thermal expansion of the sample exciting the AFM cantilever, whose thermomechanical response is proportional to the absorbed light. Scanning the cantilever on the sample while fixing the laser wavelength enables one to simultaneously obtain nanoscale-resolved a) morphology, b) chemical (IR absorption), and c) mechanical maps. d) nanoscale-localised (red cross) IR spectra are then obtained by sweeping the laser wavelength while fixing the position of the cantilever.

AFM-IR has recently been successfully exploited to study protein droplets for drug delivery purposes, to evaluate the effect of post-translational modifications, specifically methylation, and to investigate the interactions and phase-separation behaviour, in addition to the effect of shear, on liquid phase-separated condensates (Müller *et al.*, 2014; Volpatti *et al.*, 2016). In an initial study involving the application of AFM-IR to phase-separated droplets, it was shown that a change in methylation state alters the structural and biophysical state of condensates of FUS, the dysfunction of which impairs neuronal function. The study quantitatively compared the structural state of the methylated and hypomethylated condensates, showing an increased content of antiparallel β -sheet in the latter. Hypomethylated FUS also showed heterogeneity with the coexistence of liquid and gel-like states within a single condensate, suggesting a possible interconversion between the two states (Qamar *et al.*, 2018). A more recent study reported a liquid-to-solid transition through the application of shear, which led to the formation of stable fibres that were more anisotropically ordered and had a higher β -sheet content and intermolecular hydrogen bonding compared with spherical liquid-liquid phase-separated condensates (Shen *et al.*, 2020). In this study, infrared nanopolarimetry was applied to study the internal structural organisation of the shear-formed FUS fibrils.

Here, we describe the protocol followed for the controlled, in-depth characterisation of the morphology, stiffness, and chemical properties of phase-separated condensates using AFM-IR.

Materials and Reagents

1. FUS sample at a concentration of 1-10 μ M (the production and purification of FUS is discussed in previously published protocols (Qamar *et al.*, 2018))
2. ZnSe window (Thorlabs, catalog number: WG70530)
3. MilliQ water

Equipment

1. AFM-IR with thermomechanical detection: nanoIR1, nanoIR2, or nanoIR3 (Anasys Instruments, Bruker, USA)
2. PR-EX-nIR2 AFM probes: silicon, gold-coated, with a nominal radius of 30 nm and a spring constant of 0.2 N/m (for contact mode measurements; Anasys, Bruker, USA)
3. P10 Pipette (Starlabs, UK)

Software

1. In-built nanoIR software (Bruker, USA)
2. SPIP (Image Metrology, Denmark, <https://www.imagemet.com/products/spip/>)
3. OriginPRO (Origin Labs, USA, <https://www.originlab.com/origin>)

Procedure

A. Sample preparation for AFM-IR measurements

1. Pipette 10 μ l sample onto the hydrophobic ZnSe crystal. Incubate for 1 min to allow for physisorption. Longer deposition times are possible, but this may induce artefacts due to artificial self-organisation on the surface.
2. Rinse three times with 1 ml MilliQ water to remove the excess salt.
3. Dry under a gentle flow of nitrogen.

B. Infrared nanospectroscopy measurements of liquid-liquid phase-separated droplets

1. Turn on the AFM-IR system and the infrared (IR) laser. This should be done 30-60 min before measurement to allow the system to reach thermal equilibrium.
2. Open the in-built software to control the AFM-IR (Figure 3). Select **file > new** to open a new **nanoIR** file. Press the **initialise** button to start the AFM-IR system.

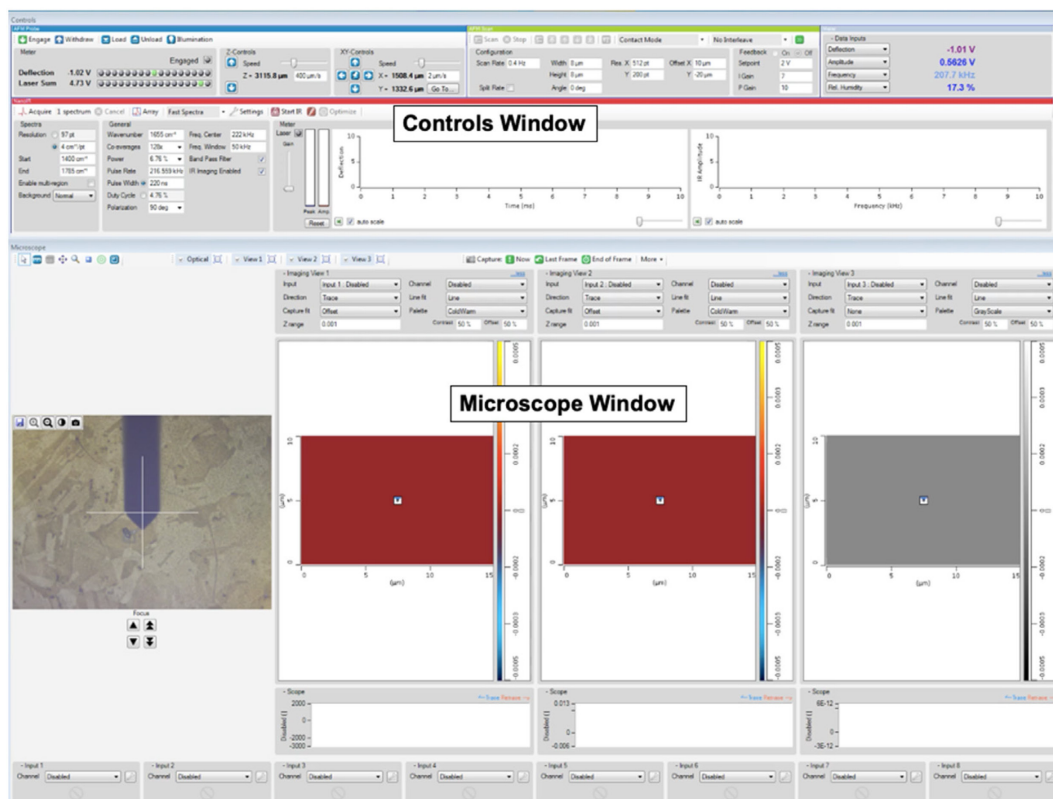


Figure 3. An overview of the nanoIR software. In the controls window, imaging parameters are given as input. In the microscope window, the relevant information is presented as imaging proceeds.

3. Open the instrument cover and mount the probe (Figure 4).

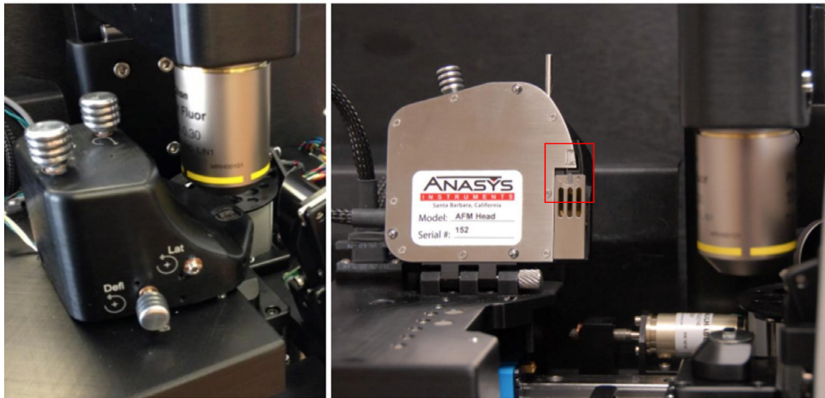


Figure 4. A photo of the AFM head. The cantilever is mounted on the AFM head (red box). Then, the knobs on the AFM head are used to adjust the position of the detection laser.

4. Now, focus the optical camera on the cantilever. Select **AFM Probe > Load > Next**. Under **focus on probe**, click on the arrows to change the focus. Under **sample XY movement**, use the arrows to position the crosshair on the cantilever.
5. Focus the detection laser on the end of the cantilever using the knobs. The value of the sum measured by the four-quadrant photodiode should be at least 3 V. Use the **deflection** knob in the AFM head and adjust the cantilever deflection to -1 V and then click **next**.
6. Close the cover of the instrument.
7. Focus the camera on the sample using the arrows under **focus on sample** (Figure 5).

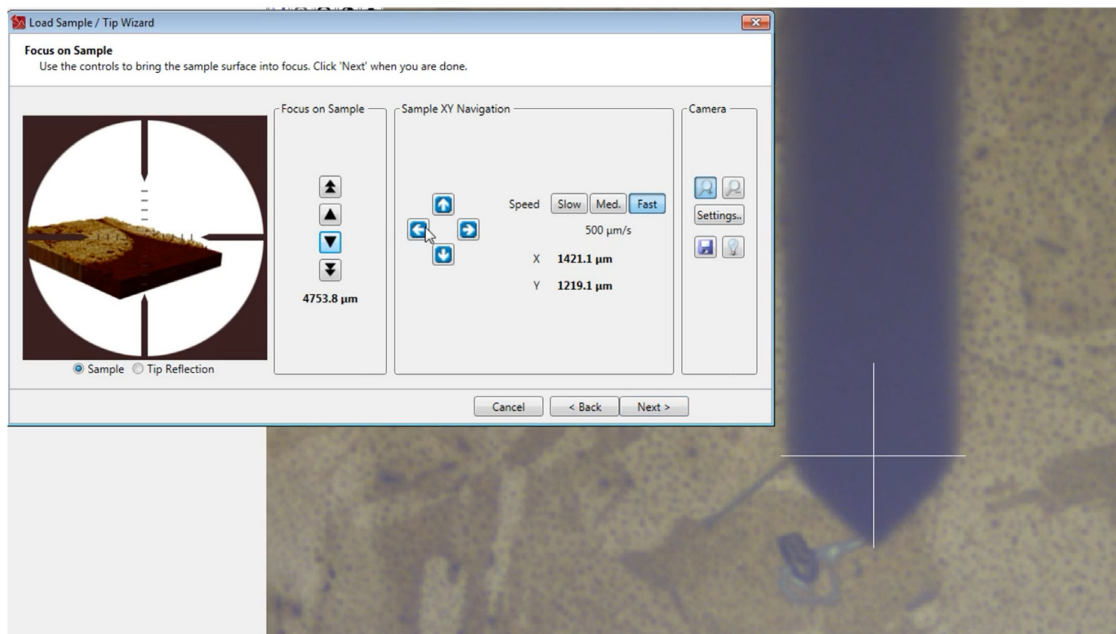


Figure 5. Illustration of Steps B4-B7. The cantilever is loaded, and the optical camera and laser focused on the end of the cantilever. Then, the camera is focused on the sample surface. Arrows can be used to navigate around the sample.

- To select a region of interest on the sample, select **sample XY movement**. Use the arrows to move around the sample surface. When you have identified the region of interest, click on **approach and engage**.
- In this context of the study of protein droplets, the information on morphology, IR absorption, and stiffness are of particular interest. To measure these parameters, select the display channels under the **microscope** window. Choose **Height** for morphology, **Amplitude 2** for IR absorption, and **PLL frequency** to map tip-sample contact resonance (Figures 6 and 7).
Note: During morphology acquisition, the tip and the sample in contact can be considered a system of coupled springs. The contact resonance of these springs is related to the intrinsic stiffness of the sample. A stiffer sample causes an increase in contact resonance, which we can term 'frequency shift.'

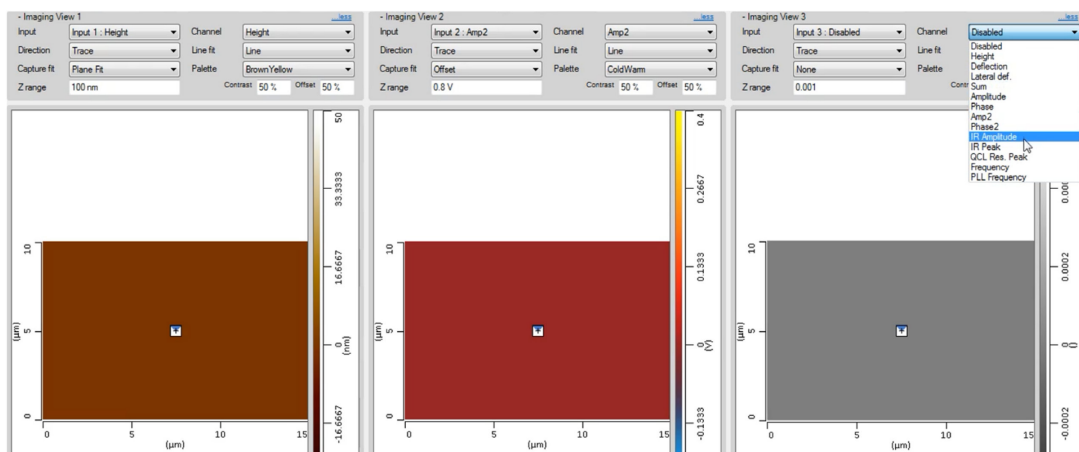


Figure 6. Demonstration of Step B9, in which display channels are selected according to the parameters of interest. In this case, they are morphology (Height), tip-sample contact resonance frequency (PLL Frequency), and IR absorption (Amp2).

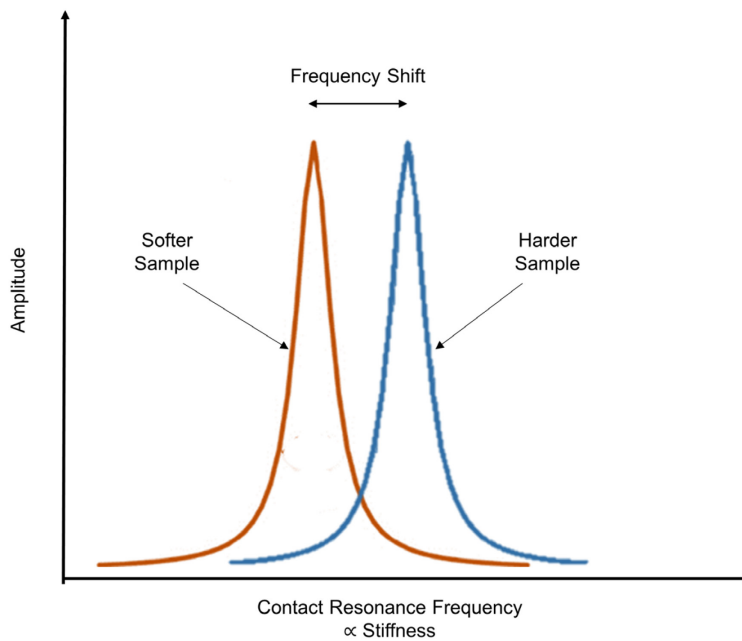


Figure 7. The contact resonance between the tip and the sample is related monotonically to the intrinsic sample stiffness. A stiffer sample causes a shift to a higher frequency, which can be used to investigate the relative stiffness of heterogeneous samples.

10. Set the imaging parameters for morphology measurements in the **AFM scan** section of the **controls** window (Figure 8).

Note: It is important to consider the sample properties when selecting imaging parameters. For example, choosing a lower scan rate will decrease the lateral force exerted on the sample, which is relevant for biological samples; however, this choice will increase the image acquisition time. A higher number of pixels will increase the image resolution but will similarly increase the image acquisition time. The gain values should be selected considering the sample roughness (i.e., a higher integral gain will allow the system to respond to changes in sample height but can also introduce noise). The following are the recommended range of values: scan rate 0.1-1.0 Hz and 256×256 - 1024×1024 pixels. The appropriate range for gain values are as follows: integral I = 1-10 and proportional P = 5-30. The value of the gains should be chosen as the minimal values to have overlapping trace and retrace scan lines.

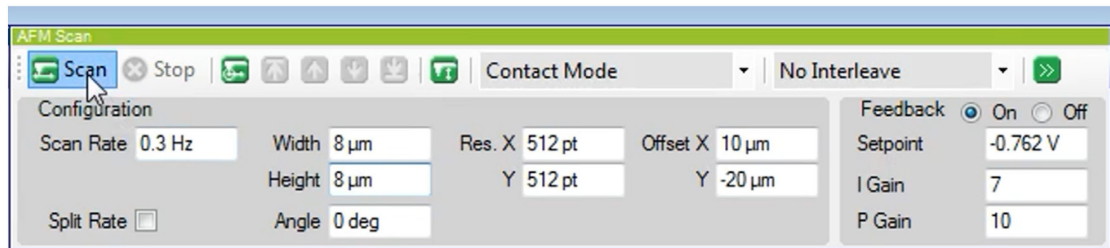


Figure 8. A demonstration of Step B10, in which the imaging parameters are input for morphology mapping. The parameters that should be considered first are the scan rate, image size, resolution (pixels), setpoint, and gain (integral and proportional).

11. Select **scan** to acquire a morphology map. Representative morphology maps and contact resonance values of FUS droplets are shown in Figures 9 and 10.

Note: The morphology can be similarly measured in dynamic tapping mode, but AFM-IR measurements are performed here in contact mode to have higher signal-to-noise ratios during infrared spectra and map acquisition.

12. When the mapping of morphology is finished (Figure 9), set up the instrument to perform the IR and contact resonance (Figure 10) measurements. In the **microscope** window, click on the height map to position the probe on top of one droplet. Then in the **nanoIR** section of the **controls** window, click on **start IR** to illuminate the sample with the IR laser.

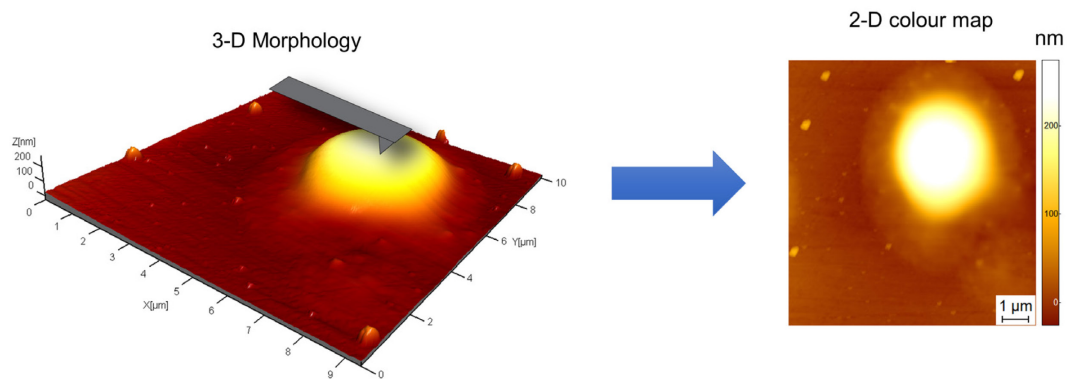


Figure 9. A representative image of the morphology of a FUS droplet. The 3D morphology of a droplet is represented as a 2D colour map, with lighter colours indicating increasing height.

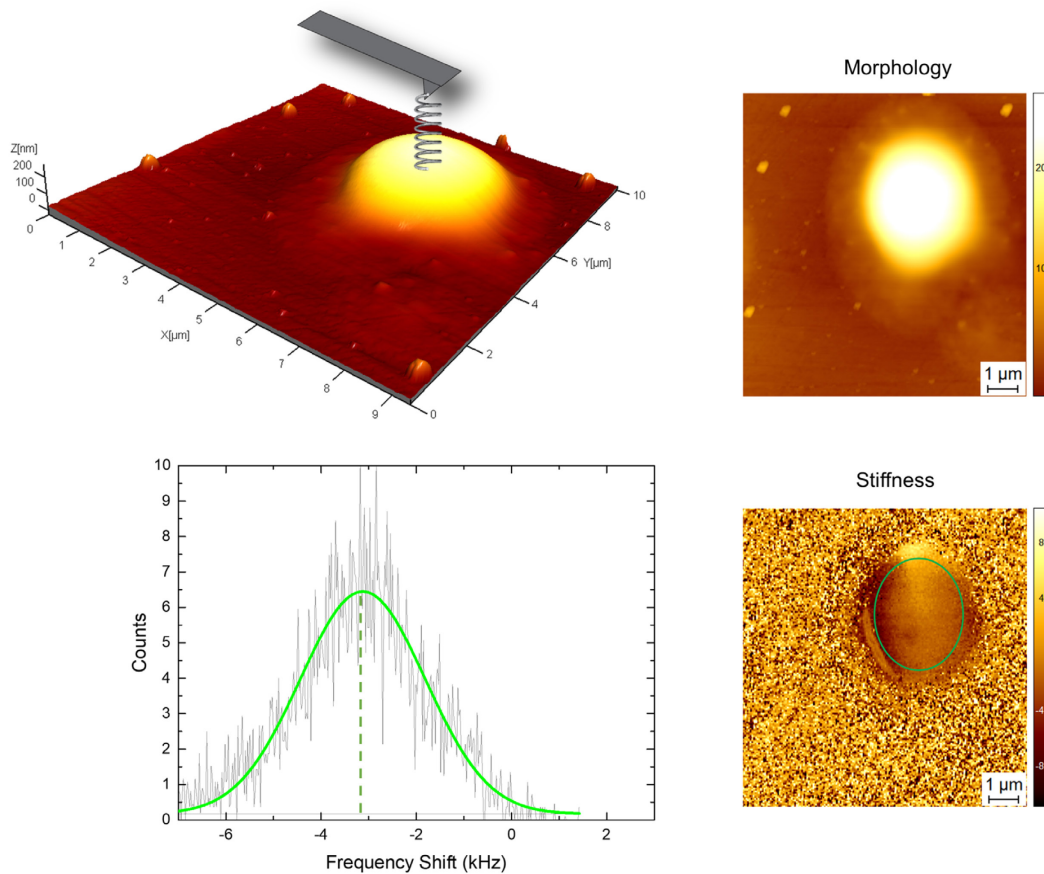


Figure 10. A representative contact resonance map of a FUS droplet. A contact frequency map is simultaneously acquired during morphology acquisition. Tip-sample contact resonance provides information regarding sample stiffness. A stiffer sample would cause an increase in contact resonance, which we can term ‘frequency shift.’

13. To focus the infrared laser on the cantilever, click on **optimisation**. In this window, write your chosen wavenumber click **add**.

Note: The wavenumber should be chosen such that your sample will have significant absorbance. If the sample absorbs IR light at a specific wavelength, chemical bonds will vibrate, causing a thermal expansion of the sample that can be detected by the AFM tip in contact with the droplet. A typical value for protein samples is $1,655\text{ cm}^{-1}$, which corresponds to the amide I band. The response of the cantilever is proportional to the absorption of IR light by the sample; thus, differences in IR absorption can be mapped and correlated to the corresponding morphology map.

14. Select **scan** to find the IR laser position and then **update** to align its position with the cantilever (Figure 11). Close the window.

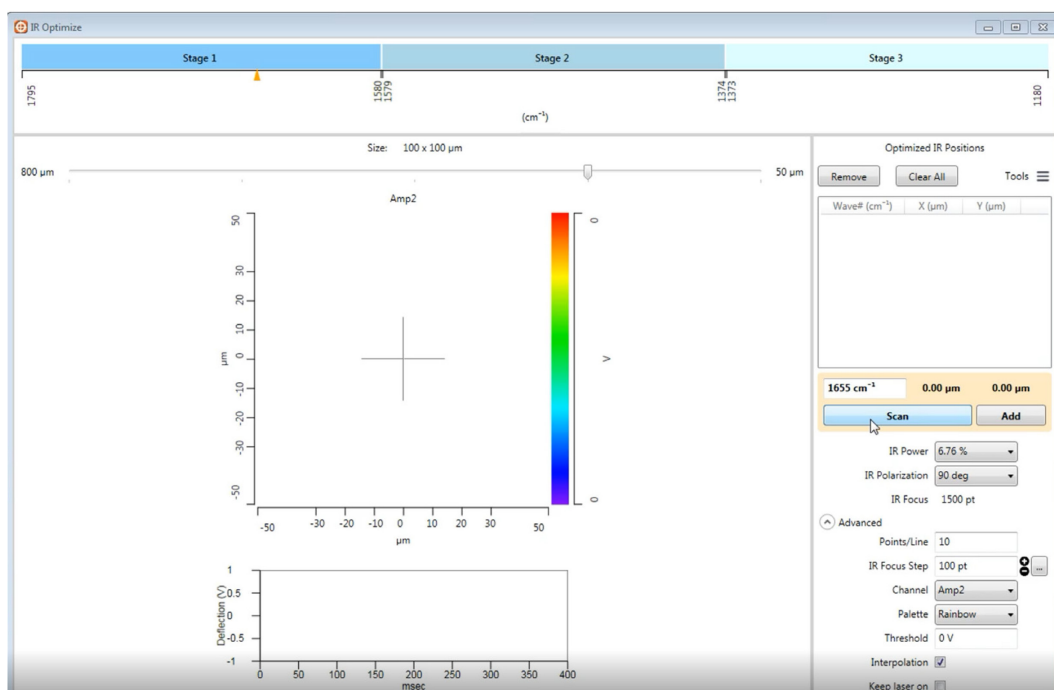


Figure 11. A demonstration of Steps B13 and B14, in which the wavenumber of interest, in this case 1,655 cm⁻¹, is entered. Then select scan to find the IR laser position and update to align its position with the cantilever.

15. Select **general** in the **nanoIR** settings. Input a wavenumber where IR absorption is expected. Then, deactivate the **Band Pass Filter** option and look at the **meter** reading and fast Fourier transform (FFT) of the cantilever response. In the FFT window, move the green cursor to read the resonance frequency of the cantilever (Figure 12). A typical value for the FFT of the resonance of the cantilevers is around 300 kHz. Write the found resonance frequency value in the **general** section of the **freq. centre** field and use a **freq. window** of 50 kHz. Select a laser power that is low enough to avoid saturating the **meter** reading, distorting the cantilever response, and overheating the sample.

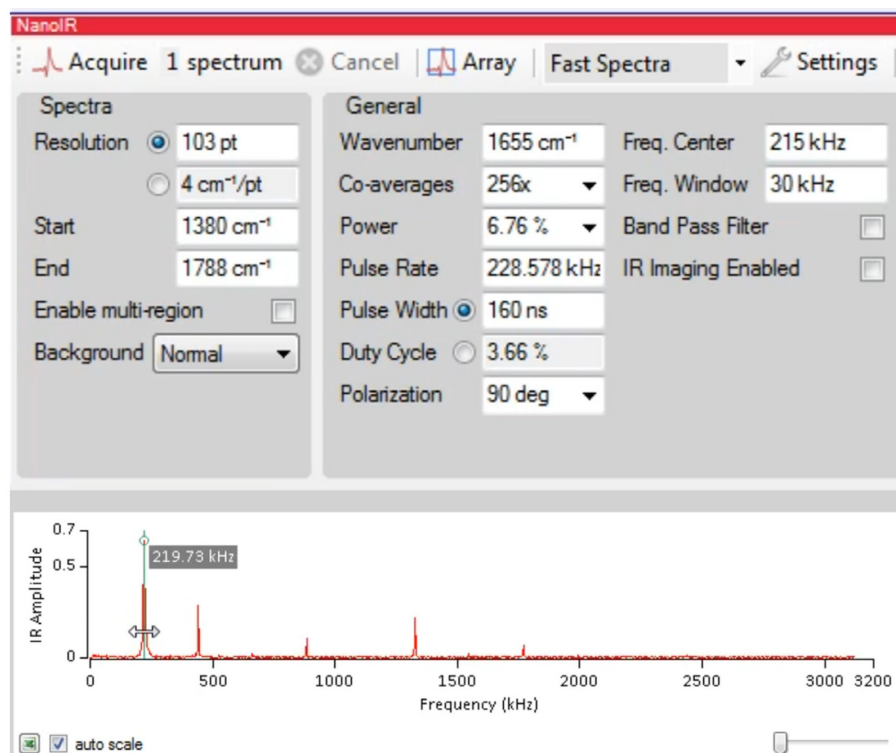


Figure 12. A demonstration of B15, in which the parameters of the IR laser are set up. On the left-hand side, input the parameters as described above. On the right-hand side, the meter reading displays the thermomechanical response of the cantilever. Use the cursors to centre the green course at the peak of the resonance frequency. Once the value for the resonance frequency has been determined, input it in the **Freq. Centre** on the left-hand side.

16. Click on the **laser pulse tune window** to use the resonance enhanced mode. Choose a frequency centre of 300 kHz, a tune range of 50 kHz, and a duty cycle of the laser of 5% (*Duty cycle* is the fraction time during which there is *laser* pulse emission). Click on **acquire** to sweep the pulse rate of the laser. Use the cursor in the graph to tune the laser pulse to the frequency of the mechanical response of the thermal expansion of the sample absorbing the IR light (Figure 13).

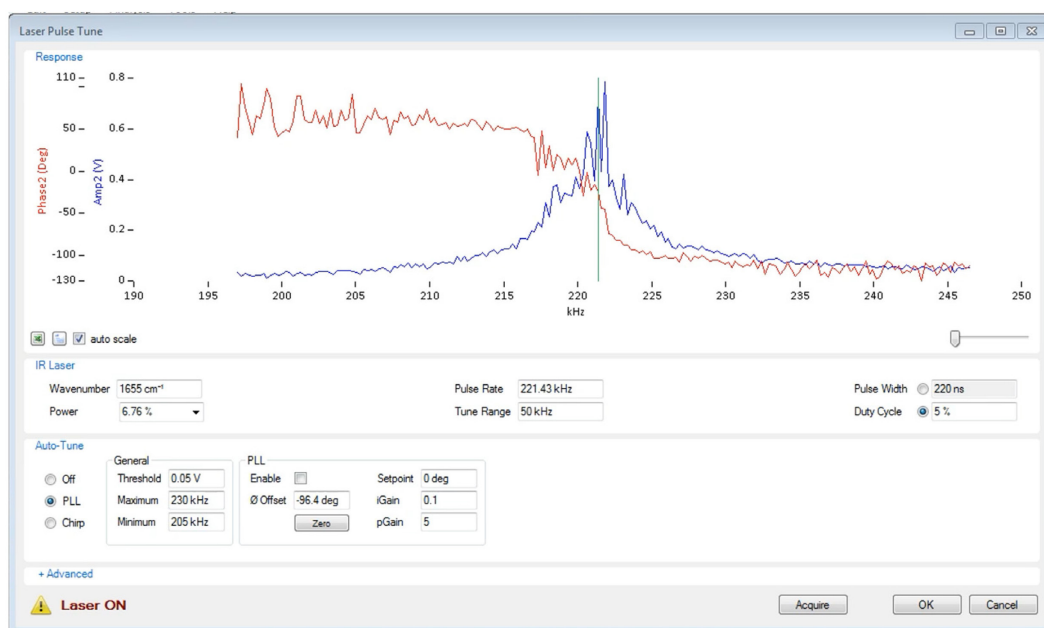


Figure 13. A demonstration of laser tuning (Steps B16 and B17). In the laser pulse tune window, input the parameters as described in Step B19. Click on **acquire** to display the contact resonance frequency and phase. Under the auto-tune window, select **PLL** to track the contact resonance frequency of the resonance enhanced mode.

17. To avoid cross-talk between the chemical and mechanical information in the sample, it is important to track the contact resonance frequency in resonance enhanced mode by a phase locked loop (PLL). Select **PLL**, then click the **zero** button in the PLL window and tick **enable**. Choose an integral gain $I = 0.5$ and proportional gain $P = 10$.
18. Open the **optimisation** window again and identify the position of the IR laser for at least 3 wavelengths corresponding to the major absorbance bands of the sample. For a protein sample, this should be amide bands I, II, and III. Moreover, identify the position of at least one wavelength for each chip of the laser.
19. Click on **Tools > IR Background Calibration > New** (Figure 14). In the window, select the spectroscopic region of interest, which is $1,800\text{-}1,200\text{ cm}^{-1}$ in the case of a protein sample. Choose the same pulse rate as determined in Step B16 and a duty cycle of 5%.

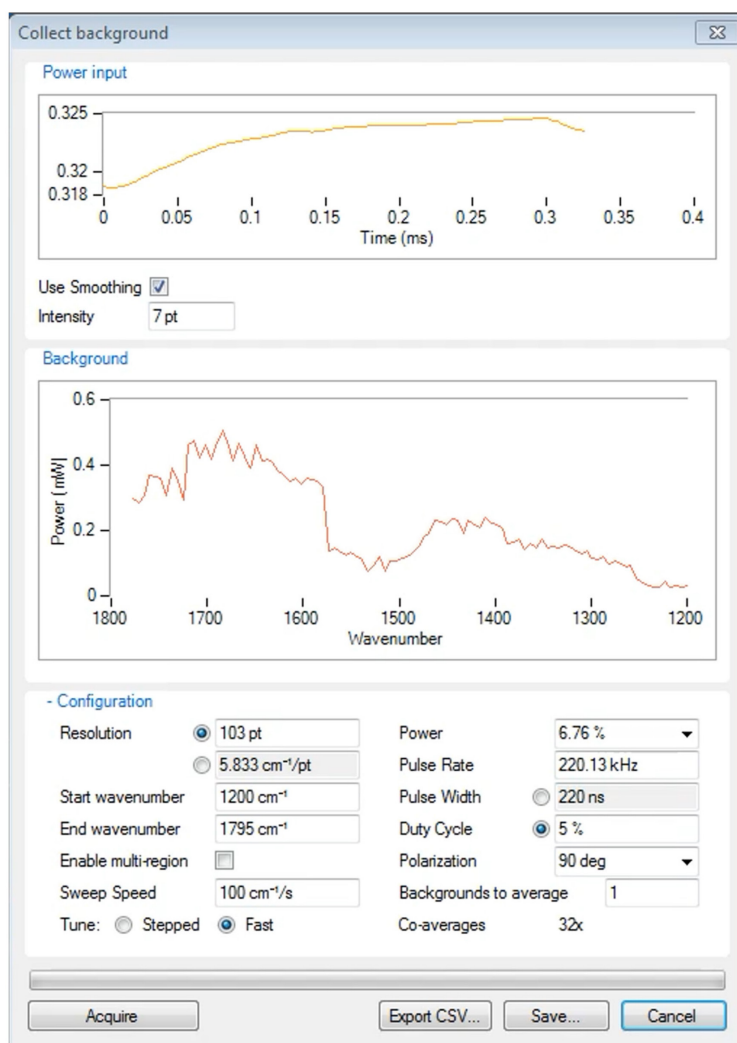


Figure 14. A demonstration of the steps for background calibration (Steps B19-B21). Input the parameters as described above. Then, select acquire to generate a spectrum of the background (*i.e.*, the substrate).

20. Select **fast** acquisition and choose the laser speed. For a quantum cascade laser, a typical range is between 20-5,000 cm^{-1}/s . The background spectrum will be used for normalisation of the measured nanoscale localised spectra. Close the window.
21. If a fast laser and resonance-enhanced mode is not available, skip Step B16 and select **stepped** spectra instead of **fast** in both the **background** and **IR spectra** acquisition windows. This will still allow for chemical characterisation. While this sensitivity is not sufficient to reach the single-molecule level, it still allows for full characterisation of liquid-liquid phase-separated droplets with a typical size ranging from hundreds of nanometers to micrometers.
22. Now, measure a nanoscale-localized IR spectrum in the protein range (1,800-1,200 cm^{-1}) (Figure 15). In the **IR spectra** settings, choose an IR spectrum resolution of 1-4 cm^{-1} . For the number of co-averages, choose at least 64. Select **acquire**.

23. Additionally, a nanoscale-resolved chemical map can be acquired (Figures 15 and 16). To do this, select the **IR imaging** option, choose a wavenumber of interest (e.g., $1,655\text{ cm}^{-1}$ for amide I), and click on **scan** in the **AFM scan** window.

Note: The principles of acquiring localised IR spectra and IR maps are generally the same. When acquiring IR maps, the tip is scanned across the sample while maintaining a fixed laser wavenumber, so that the absorption of the sample and surface is mapped at that wavenumber. When acquiring a localised spectrum, the tip is held in a fixed position on the sample, and the IR laser wavenumber is varied to obtain absorption across a range of values. This provides a full IR spectrum that can then be used to provide specific information regarding the secondary structural contributions (discussed further below).

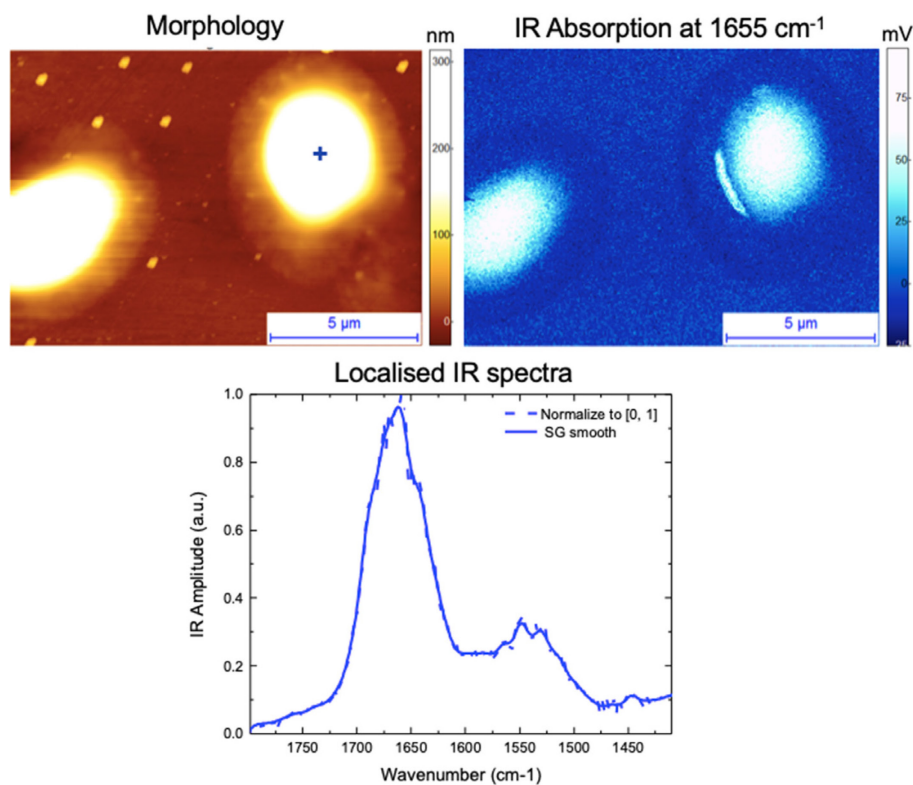


Figure 15. Representative IR map and localised IR spectra of FUS droplets. An IR absorption map can be measured simultaneously during morphology mapping (together with the contact resonance map). The localised IR spectra can also be acquired at a single point on the surface of a droplet (indicated by the blue cross).

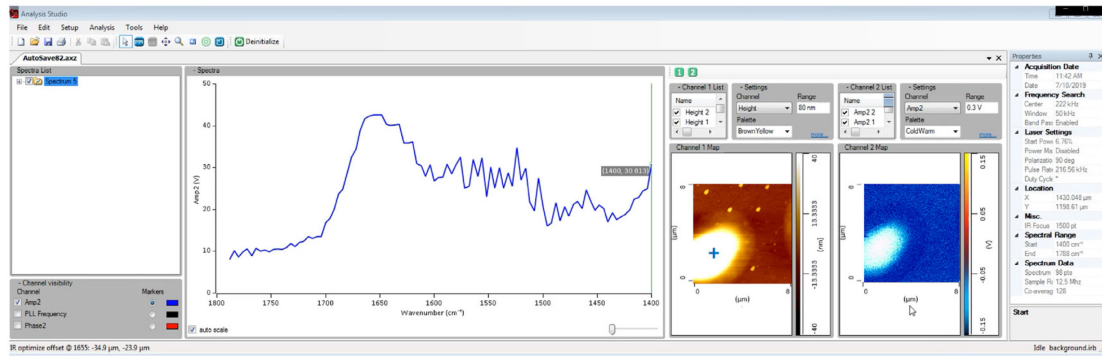


Figure 16. An example of completed raw morphology and IR maps, as well as typical raw localised IR spectra. The blue cross indicates where the localised IR spectra were recorded.

24. Our advice is to acquire multiple localised spectra within one droplet to enable appropriate statistical significance for studying its heterogeneity. Repeat Step B22 multiple times within each droplet.

C. Data processing and analysis

1. Open an imaging processing software, such as SPIP, to process AFM maps.
2. First-order flatten AFM maps by selecting **General > Plane Correction > Plane Correction Set-Up**.
3. Under **Global Correction**, select **Average Profile Fit**.
4. Select **Degree** to 0, then **Apply**.
5. Repeat for **Degree** = 1.
6. Zero-order flatten IR and stiffness-related maps by repeating the sample flattening procedure (excluding Step C2).
7. To evaluate the relative sample stiffness, consider the distribution of the values for the pixels of the contact resonance frequency to calculate its average and standard deviation inside each region of interest in your sample (Figure 8). Then, plot these averages as a normalised ratio (Figure 17). Due to the complicated nature of determining the absolute stiffness of soft droplets, the stiffness of the droplets should be considered relative to the ZnSe substrate. To prove that the measured mechanical differences are real, the mechanical differences should be evaluated for independent tips and samples. Any software of your choice can be used.

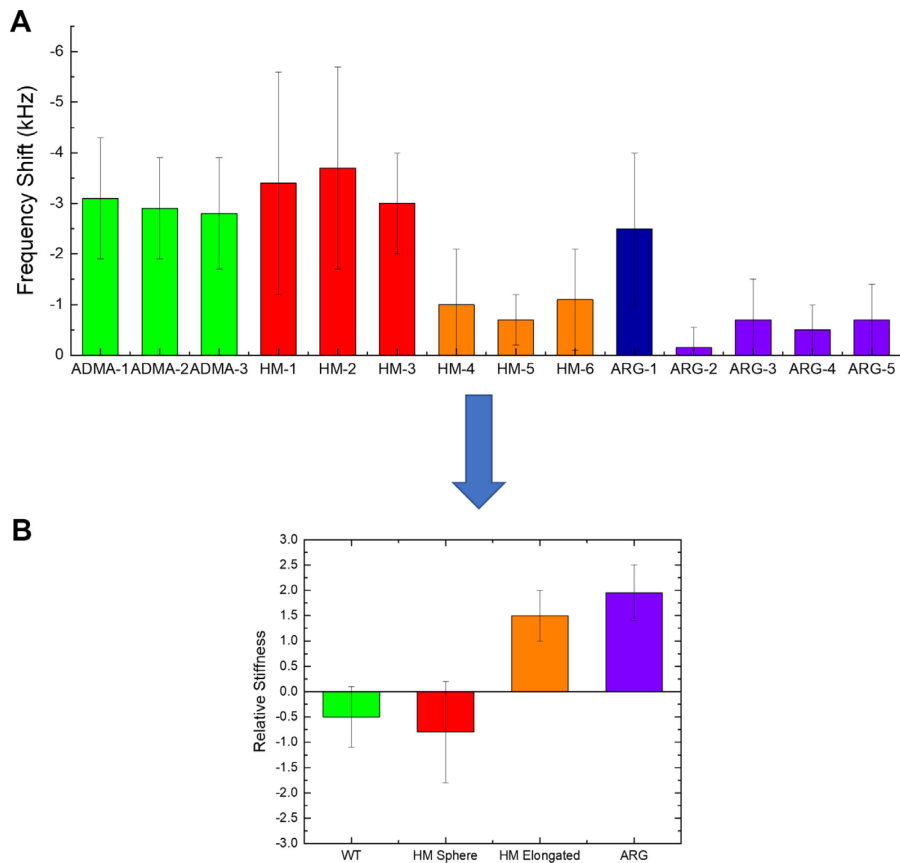


Figure 17. Measuring sample stiffness. A. An example of plotted average frequency shifts for each droplet measured. B. Relative stiffness of the droplets can be determined by representing the data as a ratio of the average frequency shifts.

- Next, IR spectra can be processed by the OriginPro software to have normalised smoothed spectra and their second derivatives (Figure 18).

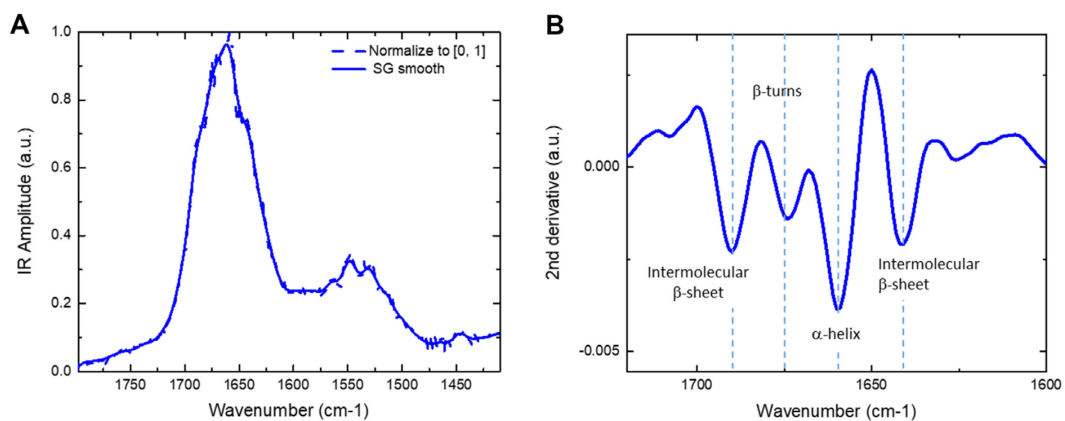


Figure 18. The second derivative of the IR spectrum provides information on the secondary structure of the droplets. A. Representative processed IR spectrum of the droplets

in the protein range (1,800-1,400 cm^{-1}). B. A second derivative operation was performed to identify the secondary structure.

9. For each spectrum acquired, subtract the spectrum acquired in a location close to the droplet on the ZnSe substrate to eliminate buffer absorption or tip contamination contributions. **Select Analysis > Data Manipulation > Reference Data.** Select the **Input1** as your droplet spectrum and the **reference data** input as your ZnSe substrate spectrum. **Select Okay.**
10. Then for each droplet or for a specific location on its area, calculate an average spectrum by averaging spectra taken at different positions within the droplet. To reduce the level of instrumental noise in the spectra, at least 5 spectra should be averaged. Select **Analysis > Mathematics > Average Multiple Curves > Open Dialogue.**
11. For **Method**, select **Average**; for **Averaged X**, select **Common X Range.**
12. Select **additional output** parameters as desired and select **Okay.**
13. Smooth the average spectrum by applying a Savitzky-Golay filter (second order, 9 points). Select **Analysis > Signal Processing > Smooth > Open Dialogue.**
14. From the drop-down list for **Method**, select **Savitzky-Golay.**
15. For **Points of Window**, input **9.**
16. For **Polynomial Order**, select **2.** Select **Okay.**
17. Next, normalise the spectrum. Select **Analysis > Mathematics > Normalise Curves > Open Dialogue.**
18. For **Normalize Methods**, select **Normalize to [0,1]**, then **Okay.**
19. Take the second derivative of the smoothed normalised spectrum. Select **Analysis > Mathematics > Differentiate.**
20. For **Derivative Order**, select **2.**
21. Under Smooth, check the box for **Savitzky-Golay Smooth.** For **Polynomial Order**, select **2;** for **Points of Window**, select **9.**
22. Tick the box for **Plot Derivative Curve** and select **Okay.**

Note: The amide I band contains information on the secondary structure, as C=O stretching is influenced by the backbone conformation. Deconvoluting the spectrum by taking the second derivative provides quantitative information on the structural contribution (i.e., provides information on the content of α -helices, β -sheets, and random coils). An example of this is shown in Figure 18.

Acknowledgments

The authors acknowledge funding from Darwin College, University of Cambridge (FSR) and Emmanuel College, University of Cambridge (AMM). This protocol was largely derived from previous work presented in Qamar *et al.* (2018).

Competing interests

The authors have no competing interests to declare.

References

1. Alberti, S., Gladfelter, A. and Mittag, T. (2019). [Considerations and Challenges in Studying Liquid-Liquid Phase Separation and Biomolecular Condensates](#). *Cell* 176(3): 419-434.
2. Banani, S. F., Lee, H. O., Hyman, A. A. and Rosen, M. K. (2017). [Biomolecular condensates: organizers of cellular biochemistry](#). *Nat Rev Mol Cell Biol* 18(5): 285-298.
3. Dazzi, A. and Prater, C. B. (2017). [AFM-IR: Technology and Applications in Nanoscale Infrared Spectroscopy and Chemical Imaging](#). *Chem Rev* 117(7): 5146-5173.
4. Hyman, A. A., Weber, C. A. and Julicher, F. (2014). [Liquid-liquid phase separation in biology](#). *Annu Rev Cell Dev Biol* 30: 39-58.
5. Li, P., Banjade, S., Cheng, H. C., Kim, S., Chen, B., Guo, L., Llaguno, M., Hollingsworth, J. V., King, D. S., Banani, S. F., Russo, P. S., Jiang, Q. X., Nixon, B. T. and Rosen, M. K. (2012). [Phase transitions in the assembly of multivalent signalling proteins](#). *Nature* 483(7389): 336-340.
6. Lipiec, E., Ruggeri, F. S., Benadiba, C., Borkowska, A. M., Kobierski, J. D., Miszczyk, J., Wood, B. R., Deacon, G. B., Kulik, A., Dietler, G. and Kwiatek, W. M. (2019). [Infrared nanospectroscopic mapping of a single metaphase chromosome](#). *Nucleic Acids Res* 47(18): e108-e108.
7. Müller, T., Ruggeri, F. S., Kulik, A. J., Shimanovich, U., Mason, T. O., Knowles, T. P. J. and Dietler, G. (2014). [Nanoscale spatially resolved infrared spectra from single microdroplets](#). *Lab on a Chip* 14(7): 1315-1319.
8. Murakami, T., Qamar, S., Lin, J. Q., Schierle, G. S., Rees, E., Miyashita, A., Costa, A. R., Dodd, R. B., Chan, F. T., Michel, C. H., Kronenberg-Versteeg, D., Li, Y., Yang, S. P., Wakutani, Y., Meadows, W., Ferry, R. R., Dong, L., Tartaglia, G. G., Favrin, G., Lin, W. L., Dickson, D. W., Zhen, M., Ron, D., Schmitt-Ulms, G., Fraser, P. E., Shneider, N. A., Holt, C., Vendruscolo, M., Kaminski, C. F. and St George-Hyslop, P. (2015). [ALS/FTD Mutation-Induced Phase Transition of FUS Liquid Droplets and Reversible Hydrogels into Irreversible Hydrogels Impairs RNP Granule Function](#). *Neuron* 88(4): 678-690.
9. Patel, A., Lee, H. O., Jawerth, L., Maharana, S., Jahnel, M., Hein, M. Y., Stoykov, S., Mahamid, J., Saha, S., Franzmann, T. M., Pozniakovski, A., Poser, I., Maghelli, N., Royer, L. A., Weigert, M., Myers, E. W., Grill, S., Drechsel, D., Hyman, A. A. and Alberti, S. (2015). [A Liquid-to-Solid Phase Transition of the ALS Protein FUS Accelerated by Disease Mutation](#). *Cell* 162(5): 1066-1077.
10. Patel, A., Malinowska, L., Saha, S., Wang, J., Alberti, S., Krishnan, Y. and Hyman, A. A. (2017). [ATP as a biological hydrotrope](#). *Science* 356(6339): 753-756.
11. Qamar, S., Wang, G., Randle, S. J., Ruggeri, F. S., Varela, J. A., Lin, J. Q., Phillips, E. C.,

- Miyashita, A., Williams, D., Strohl, F., Meadows, W., Ferry, R., Dardov, V. J., Tartaglia, G. G., Farrer, L. A., Kaminski Schierle, G. S., Kaminski, C. F., Holt, C. E., Fraser, P. E., Schmitt-Ulms, G., Klenerman, D., Knowles, T., Vendruscolo, M. and St George-Hyslop, P. (2018). [FUS Phase Separation Is Modulated by a Molecular Chaperone and Methylation of Arginine Cation- \$\pi\$ Interactions](#). *Cell* 173(3): 720-734 e715.
12. Ramer, G., Ruggeri, F. S., Levin, A., Knowles, T. P. J. and Centrone, A. (2018). [Determination of Polypeptide Conformation with Nanoscale Resolution in Water](#). *ACS Nano* 12(7): 6612-6619.
 13. Ruggeri, F. S., Habchi, J., Cerreta, A. and Dietler, G. (2016b). [AFM-Based Single Molecule Techniques: Unraveling the Amyloid Pathogenic Species](#). *Curr Pharm Des* 22(26): 3950-3970.
 14. Ruggeri, F. S., Habchi, J., Chia, S., Vendruscolo, M. and Knowles, T. P. J. (2020b). [Infrared nanospectroscopy reveals the molecular interaction fingerprint of an aggregation inhibitor with single A \$\beta\$ 42 Oligomers](#). *bioRxiv*: 2020.2006.2024.168997.
 15. Ruggeri, F. S., Longo, G., Faggiano, S., Lipiec, E., Pastore, A. and Dietler, G. (2015). [Infrared nanospectroscopy characterization of oligomeric and fibrillar aggregates during amyloid formation](#). *Nat Commun* 6(1): 7831.
 16. Ruggeri, F. S., Mannini, B., Schmid, R., Vendruscolo, M. and Knowles, T. P. J. (2020a). [Single molecule secondary structure determination of proteins through infrared absorption nanospectroscopy](#). *Nat Commun* 11(1): 2945.
 17. Ruggeri, F. S., Marcott, C., Dinarelli, S., Longo, G., Girasole, M., Dietler, G. and Knowles, T. P. J. (2018). [Identification of Oxidative Stress in Red Blood Cells with Nanoscale Chemical Resolution by Infrared Nanospectroscopy](#). *Int J Mol Sci* 19(9).
 18. Ruggeri, F. S., Vieweg, S., Cendrowska, U., Longo, G., Chiki, A., Lashuel, H. A. and Dietler, G. (2016a). [Nanoscale studies link amyloid maturity with polyglutamine diseases onset](#). *Sci Rep* 6: 31155.
 19. Shen, Y., Ruggeri, F. S., Vigolo, D., Kamada, A., Qamar, S., Levin, A., Iserman, C., Alberti, S., George-Hyslop, P. S. and Knowles, T. P. J. (2020). [Biomolecular condensates undergo a generic shear-mediated liquid-to-solid transition](#). *Nat Nanotechnol* 15(10): 841-847.
 20. Volpatti, L. R., Shimanovich, U., Ruggeri, F. S., Bolisetty, S., Müller, T., Mason, T. O., Michaels, T. C. T., Mezzenga, R., Dietler, G. and Knowles, T. P. J. (2016). [Micro- and nanoscale hierarchical structure of core-shell protein microgels](#). *J Mater Chem B* 4(48): 7989-7999.